Strongly Correlated Electrons and High Temperature Superconductivity

Takashi Yanagisawa

National Institute of Advanced Industrial Science and Technology, Electronics and Photonics Research Institute, Advanced Engineering Research Institute, 1-1-1 Umezono, Tsukuba, Ibaraki 305-8568, Japan

* Corresponding author. E-mail: t-yanagisawa@aist.go.jp

ABSTRACT: It is very important to clarify the mechanism of high-temperature superconductivity in strongly correlated electron systems. The mechanism of superconductivity in high temperature cuprate superconductors has been studied extensively since their discovery. We investigate the properties of correlated electron systems and mechanism of superconductivity by using the optimization quantum variational Monte Carlo method. The many-body wave function is constructed by multiplying by correlation operators of exponential type. We show that *d*-wave superconducting phase exists in the strongly correlated region where the on-site repulsive interaction is as large as the bandwidth or more than the bandwidth. The *d*-wave pairing correlation function is shown as a function of lattice sites, showing that the long-range order indeed exists.

Keywords: high-temperature superconductivity; strongly correlated electron systems; mechanism of superconductivity; optimization variational Monte Carlo method; Hubbard model; phase diagram

1. Introduction

The physics of high-temperature superconductors have been studied intensively for more than 35 years since the discovery of high-temperature superconductivity [1]. It is still a challenging issue to clarify the mechanism of high-temperature superconductivity. Since the parent materials of high-temperature cuprates are Mott insulators when no carriers are doped, high-temperature cuprates are typical strongly correlated electron systems. The strong correlation makes it hard to elucidate the mechanism of superconductivity. Thus, it is important to understand the electronic properties of strongly correlated electron systems.

The CuO_2 plane is commonly contained in various high temperature cuprates and consists of oxygen atoms and copper atoms. It is certain that the CuO_2 plane plays an important role in the emergence of high-temperature superconductivity [2-8]. The fundamental and important model on this plane is the three-band d-p model [4-26]. The two-dimensional (2D) Hubbard model is regarded as an effective model where we consider only *d* electrons by integrating out the freedom of *p* electrons. The 2D Hubbard model [27-29] is also the basic model for cuprate superconductors.

The 2D Hubbard model contains fruitful physics although it looks very simple, and it may include effective interactions that induce electron pairing to bring about high-temperature superconductivity. The Hubbard model has been studied intensively to clarify the pairing mechanism of high-temperature superconductivity [30-49]. One may wonder why the effective attraction arises between electrons from the on-site repulsive Coulomb interaction. This effective pairing interaction may originate from the effective nearest-neighbor exchange coupling and the kinetic energy effect. On this subject the ladder Hubbard model (two-chain model) has also been studied [50-55].

The Hubbard model was first introduced to understand the metal-insulator transition [27]. Recent studies indicate the possibility of existence of superconducting (SC) phase in the parameter space of the hole density, the strength of Coulomb interaction U and next nearest-neighbor transfer integral t' in the ground state [47]. These three parameters are important and give plentiful structures of the phase diagram that include superconducting phase and antifer-

romagnetic phase. The transfer t' plays an essential role in determining the stability of magnetic states. For example, in the case where $t' = 0$, the antiferromagnetic state becomes unstable when holes are doped. The 2D Hubbard model is also useful to understand the appearance of inhomogeneous electronic states such as stripes [56-71] and checkerboard-like density of states [72-75]; the existence of these inhomogeneous states has been indeed reported for high-temperature cuprates.

In the study of cuprate superconductors and also iron-based superconductors, lattice and charge effects play an important role. Inhomogeneous striped states could be stabilized associated with lattice distortions [62]. Many interesting properties have been reported concerning lattice effects such as an anomalous isotope effect [76-79] and a shape resonance in a superlattice of quantum strings [80, 81]. In the study of cuprate superconductors $Bi_2Sr_2CaCuO_{8+y}$ and La_2CuO_{4+y} for which mobile oxygen interstitials by using local probes, a scenario has been shown that a strongly correlated Fermi liquid coexists with stripes which are made of anisotropic polarons condensed into a generalized Wigner charge density wave [82-84].

The relation between the Hubbard model and the d-p model was investigated in the early state of the study of high-temperature cuprates by Feiner et al. [85] They were able to reduce the d-p model into an effective one-band model by means of the cell-perturbation method. It has also been shown by numerical calculations that the Hubbard model and the three-band d-p model exhibit similar electronic properties [14, 26].

In order to explore the superconducting ground state, it is favorable to suppress magnetic correlations and magnetic instabilities. For this purpose, we consider the strongly correlated region with large U. The strong antiferromagnetic correlation is suppressed by doped hole carriers when U is large. In this region we calculated superconducting properties in the 2D Hubbard model, and the existence of superconducting phase is followed.

In section 2 we discuss the critical temperature of superconductivity in many-electron systems. We discuss improved many-body wave functions in section 3. In section 4, we show the results obtained by the optimization variational Monte Carlo method. We show the SC order parameter as a function of U and phase diagrams when we vary the hole density x. We discuss the kinetic energy driven superconductivity in the strongly correlated region. We also examine the possibility of superconductivity in nematic charge-ordered phase. In section 5, we exhibit pair correlation function as a function of lattice sites. This shows that the pair correlation function is almost constant at long distances and the wave function indeed has long-range superconducting order in the strongly correlated region. We also discuss the duality of strong electron correlation, which means that the strong correlation can be an origin of attractive interaction of d-wave electron pairs and at the same time, it suppresses pair correlation function.

2. Superconductivity in many-electron systems

It is reasonable to expect that when the energy scale of an interaction is very large, we can expect superconductivity with high critical temperature T_c. Since the energy scale of the Coulomb interaction is of the order of eV, the Coulomb interaction is one of candidates to give high-temperature superconductivity. For materials shown in Table 1, we can confirm that the following empirical relations holds for the superconducting critical temperature:

$$k_B T_c \simeq 0.1\, t/(m^*/m_0), \tag{1}$$

where t denotes the transfer integral, and m^* and m_0 are the effective mass and bare mass of electrons, respectively. The Table 1 shows typical values of t, the ratio m^*/m_0 and T_c. The order of T_c for correlated electron materials is consistent with the formula in Eq. (1). For high-temperature cuprates, the transfer integral t is estimated as $t\sim0.51$eV and T_C is of the order of 100K. Since the transfer t of iron pnictides is about five times smaller than that of cuprates, iron pnictides have lower T_c than cuprate superconductors. The critical temperature T_c of heavy fermions is very low although heavy fermion materials are strongly correlated electron systems. This is due to large effective mass of f electrons which is as large as 100 ~ 1000 times the band (bare) mass m_0. Then the characteristic energy scale is reduced considerably so that T_c is of the order of 1K

Table 1. The transfer integral *t*, effective mass ratio m^*/m_0 and critical temperature T_c in correlated electron systems. For Hydrides, the Debye frequency ω_{ln} is shown instead of *t*. For heavy fermion materials, $t/(m^*/m_0)$ corresponds to the Kondo temperature T_K.

	t	m^*/m_0	$t/(m^*/m_0)$	T_c	References
Cuprate superconductors	5000K	5	1000	100K	[85]
Iron pnictides	1000K	~2	500	50K	[86]
Heavy fermion materials	10,000K	100~1000	10~100	1~10K	[87-89]
Organic superconductors	200~500K	2~5	100	10K	[90]
	ω_{ln}	m^*/m_0	$\omega_{ln}/(m^*/m_0)$	T_c	Reference
Hydrides H_3S	1000K	~1	1000	100K	[91]

3. Optimization variational Monte Carlo method

3.1 Hamiltonian

We consider the two-dimensional Hubbard model that is one of simplest model in correlated electron systems. The Hamiltonian is given by

$$H = \sum_{ij\sigma} t_{ij} c_{i\sigma}^{\dagger} c_{j\sigma} + U \sum_{i} n_{i\uparrow} n_{i\downarrow}, \tag{2}$$

where t_{ij} indicates the transfer integral which takes the value $t_{ij} = -t$ when *i* and *j* are nearest-neighbor pairs and $t_{ij} = -t'$ when *i* and *j* are next nearest-neighbor pairs. *U* denotes the strength of the on-site repulsive Coulomb interaction. The energy is measured in units of *t* throughout this paper.

3.2 Many-body wave functions

3.2.1 Optimized many-body wave functions

The wave function of non-interacting many fermions is written as a Slater determinant. In a weakly interacting many-fermion system, the wave function shows a deviation from the simple Slater determinant. In many-fermion systems with strong interaction between fermions, we should consider strong correlation in many-body wave functions. For the Hubbard Hamiltonian with large interaction *U*, one convincing way to construct many-fermion wave function is to start from the Gutzwiller wave function. The Gutzwiller wave function is written as

$$\psi_G = P_G \psi_0 , \tag{3}$$

where ψ_0 is one-particle state given by a Slater determinant and P_G denotes the Gutzwiller operator that is given as

$$P_G = \prod_j \left(1 - (1-g) n_{j\uparrow} n_{j\downarrow}\right) \tag{4}$$

Where g is the variational parameter in the range of $0 \le g \le 1$. We usually take ψ_0 as the Fermi sea, the BCS wave function or a state with some magnetic or charge orders.

The Gutzwiller wave function can be improved by several ways. One is the well-known Jastrow function; this is written as

$$\psi_J = P_J P_G \psi_0, \tag{5}$$

where the Jastrow operator P_J is given by

$$P_J = \prod_j \left(1 - (1-\eta) \prod_\tau \left[d_j (1 - e_{j+\tau}) + e_j (1 - d_{j+\tau}) \right] \right), \tag{6}$$

where d_j is the operator for the doubly occupied site (so called doublon operator) given by $d_j = n_{j\uparrow} n_{j\downarrow}$, and e_j is that for the empty site (holon operator) given as $e_j = (1 - n_{j\uparrow})(1 - n_{j\downarrow})$. τ runs over all nearest-neighbor sites j. η is introduced as the variational parameter in the range of $0 \leq \eta \leq 1$.

The other effective way to improve the wave function is to multiply by the exponential operator $e^{-\lambda K}$ [46, 47,48, 92-97]:

$$\psi_\lambda = e^{-\lambda K} P_G \psi_0 = e^{-\lambda K} \psi_G, \tag{7}$$

where K is the non-interacting part of the Hamiltonian, which is called the kinetic operator in this paper, and is given by

$$K = \sum_{ij\sigma} t_{ij} c_{i\sigma}^\dagger c_{j\sigma}. \tag{8}$$

The variational parameter λ is introduced to minimize the expectation value of the ground-state energy. This wave function can be improved further by multiplying by the Gutwiller operator and the kinetic operator again [46, 93]:

$$\psi_\lambda^{(2)} = P_G(g') e^{-\lambda K} P_G(g) \psi_0 = P_G(g') \psi_\lambda, \tag{9}$$

$$\psi_\lambda^{(3)} = e^{-\lambda' K} P_G(g') e^{-\lambda K} P_G(g) \psi_0 = e^{-\lambda' K} P_G(g') \psi_\lambda, \tag{10}$$

where $P_G(g')$ is the Gutzwiller operator with variational parameter g'. λ' and g' are in general different from λ and g, respectively. We have correlated wave functions ψ_G, $\psi_\lambda^{(1)} \equiv \psi_\lambda$, $\psi_\lambda^{(2)}$, $\psi_\lambda^{(3)}$, and it is possible to generalize further.

We discuss the stability of superconducting state and magnetically ordered states by using this kind of improved and optimized wave functions. We can also discuss the metal-insulator transition on the basis of this wave function where the strong correlation between electrons plays an essential role [97].

3.2.2 Correlated superconducting wave function

The correlated superconducting state is formulated starting from the BCS wave function. The BCS wave function is written as

$$\psi_{BCS} = \prod_k \left(u_k + v_k c_{k\uparrow}^\dagger c_{-k\downarrow}^\dagger \right) |0\rangle. \tag{11}$$

The coefficients u_k and v_k appear in the ratio $u_k / v_k = \Delta_k / \left(\xi_k + \sqrt{\xi_k^2 + \Delta_k^2} \right)$ with the gap function Δ_k and $\xi_k = \epsilon_k - \mu$ where μ is the chemical potential. For the *d*-wave paring, we take $\Delta_k = \Delta_s (\cos k_x - \cos k_y)$. We usually first consider the BCS state with the Gutzwiller operator given by

$$\psi_{G-BCS} = P_{N_e} P_G \psi_{BCS}, \tag{12}$$

where P_{N_e} stands for the operator that extracts the state with N_e electrons. This wave function was referred to as the resonating valence bond state (RVB) by Anderson [98].

In our formulation the correlated superconducting wave function is given as

$$\psi_{\lambda-BCS} = e^{-\lambda K} P_G \psi_{BCS}. \tag{13}$$

In this wave function the operator P_{N_e} is not used because of the numerical method to evaluate expectation values, while in the Gutzwiller BCS state ψ_{G-BCS}, the total number of electrons is fixed. Because we use the auxiliary filed method in a Monte Carlo simulation [46, 99], we perform the electron-hole transformation for down-spin electrons:

$d_k = c^\dagger_{-k\downarrow}$, $d^\dagger_k = c_{-k\downarrow}$, and the operator for up-spin electrons remains the same [93]. We put $c_k = c_{k\uparrow}$ and $c^\dagger_k = c^\dagger_{k\uparrow}$. The electron-pair operator $c^\dagger_{k\uparrow}c^\dagger_{-k\downarrow}$ is transformed to the mixing operator $c^\dagger_k d_k$. This transformation indicates that $c_i = c_{i\uparrow}$ and $d_i = c^\dagger_{i\downarrow}$ in the real space representation. In the real space, the d-wave anisotropic pairing order parameters are assigned to each bond between the site i and its nearest-neighbor sites $i + \hat{x}$ and $i + \hat{y}$ where $\hat{x}$ and $\hat{y}$ denote the unit vectors in the $\hat{x}$ and $\hat{y}$ directions, respectively. We assign the following order parameter in the real space representation:

$$\Delta_{i,i+\hat{x}} = \Delta_s, \qquad \Delta_{i,i+\hat{y}} = -\Delta_s. \tag{14}$$

3.2.3 $e^{-\lambda K}$ and the renormalization of high-energy excitations

Let us discuss the role of $e^{-\lambda K}$ introduced in improved wave functions. It is easily seen that the operator $e^{-\lambda K}$ suppresses the weight of high-energy excitation modes because $e^{-\lambda K}$ becomes small for high-energy states. Thus $e^{-\lambda K}$ plays a role like the projection operator that projects out low-lying excitation modes. This means that the role of $e^{-\lambda K}$ is analogous to that of the renormalization group procedure, where the cutoff Λ is reduced to $\Lambda - d\Lambda$, the states near the Fermi surface are magnified and their contributions increase [100]. The parameter λ controls contributions from high-energy modes, which magnifies the states near the Fermi surface.

4. Phase diagram by the optimization variational Monte Carlo method

4.1 Superconductivity and antiferromagnetic state

In this section, we discuss possible phases of the 2D Hubbard model including superconducting and antiferromagnetic states when we vary the strength of the Coulomb interaction *U*. First, we show the result obtained by using the BCS-Gutzwiller wave function. The ground-state energy has a minimum at finite Δ_s for the BCS-Gutzwiller function with *d*-wave symmetry in the 2D Hubbard model [35, 36]. The SC condensation energy E_{cond} per site was evaluated in the limit of large system size $N \to \infty$ (where N is the number of sites). We obtained in this limit

$$E_{cond}/N \simeq 0.2\text{meV}. \tag{15}$$

Here we set $t = 0.5$eV. We obtained the similar result for the three-band d-p model [19]. This indicates that the SC condensation energy per atom is approximately given by 0.2meV which is of the order of 10^{-4}eV. In experiments, the condensation energy was estimated based on the result of specific heat measurements for YBCO [35, 101]. The result is

$$E_{cond}/N_{atom} \simeq 0.17 - 0.26\text{eV} \tag{16}$$

per Cu atom. We obtain the similar value of the condensation energy from the data of critical magnetic field [102]. Hence, we have a remarkable agreement between theoretical evaluations and experimental measurements. We can say that the characteristic energy scale of cuprate high-temperature superconductors is given by this value.

We turn to the results obtained by the improved wave function ψ_λ. We show the antiferromagnetic and superconducting order parameters as a function of *U/t* in Fig. 1 where calculations were carried out for the 2D Hubbard model on a 10×10 lattice with $t' = 0$ and $N_e = 88$. The characteristic feature of the 2D Hubbard model is that the antiferromagnetic (AF) correlation is strong and the AF state is easily stabilized when *U* is moderately large. We have also the SC phase when *U* is as large as the bandwidth or larger than it. When $t' = 0$, the AF correlation weakens upon carrier doping, and it vanishes when *U* is very large around $U/t \simeq 18$ for the hole density $x = 0.12$. The SC phase can exist as a pure *d*-wave state when *U/t* is about 18.

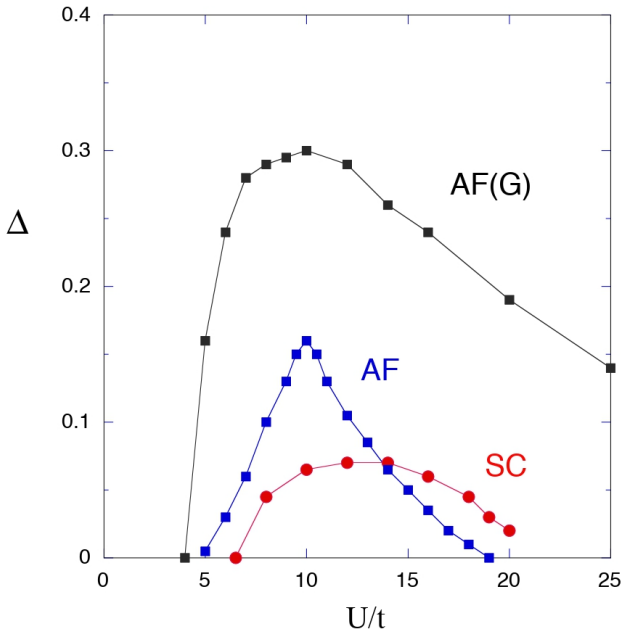

Figure 1. Antiferromagnetic and superconducting order parameters as a function of U/t where $t' = 0$ and $N_e = 88$ for the 2D Hubbard model on a 10×10 lattice (figure from [47] with a slight modification). Δ indicates the AF order parameter Δ_{AF} or the SC order parameter Δ_s. We impose the periodic boundary condition in one direction and antiperiodic boundary condition in the other direction. AF(G) indicates the result obtained by using the Gutzwiller function. The results AF and SC show those for the improved wave function ψ_λ.

The next nearest-neighbor transfer t' plays a significant role concerning the stability of the AF state. In Fig. 2 we show the AF condensation energy as a function of the hole doping rate x for the 2D Hubbard model on a 10×10 lattice. The AF condensation energy is defined as $\Delta E_{AF} = E(\Delta_{AF}= 0) - E(\Delta_{AF,\mathrm{opt}})$ where Δ_{AF} is the AF order parameter and $\Delta_{AF,\mathrm{opt}}$ is its optimized value. In the case of vanishing t', ΔE_{AF} vanishes at $x = 0.1$ when U is greater than $14t$ (Fig. 2(a)), while ΔE_{AF} remains finite (positive value) even for large U and large carrier density when $t' = -0.2$ (Fig. 2(b)). The instability of AF state for $t' = 0$ is closely related to the kinetic energy of electrons (holes). Since the kinetic energy gain in the AF state is suppressed as U increases, the total energy lowering due to the AF ordering and kinetic energy gain will get smaller for large U. Then, in order to lower the ground-state energy, the AF order will be suppressed to increase the kinetic energy gain. Finally, the AF order disappears when U becomes as large as the critical value. This is the mechanism of vanishing AF order in the strongly correlated region.

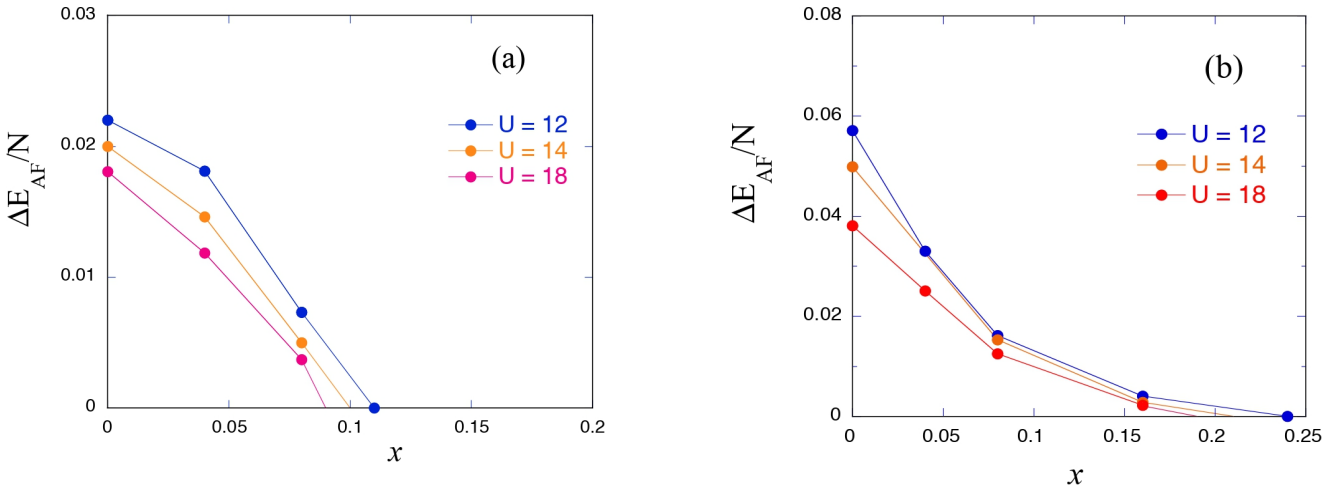

Figure 2. The AF condensation energy ΔE_{AF} per site as a function of the doping rate x for several values of U/t (where U/t = 12, 14 and 18) on a 10×10 lattice. We put (a) $t' = 0$ and (b) $t' = -0.2t$ [48].

4.2 Phase diagram

We consider the SC condensation energy defined by $\Delta E_{SC} = E(\Delta_s = 0) - E(\Delta_{s,\mathrm{opt}})$ where $\Delta_{s,\mathrm{opt}}$ is the optimized value of Δ_s to give the lowest ground-state energy. In Fig. 3, ΔE_{SC} and ΔE_{AF} are shown as a function of the doping rate x for $U/t = 18$ and $t' = 0$ on a 10×10 lattice. In the low doping region, there is the AF insulating (AFI) phase for $0 \leq x \lesssim 0.06$. The AFI is an insulating phase because of an instability toward the phase separation where the charge susceptibility χ_c becomes negative. χ_c is defined as

$$\frac{1}{\chi_c} = \frac{\partial^2 E(N_e)}{\partial N_e^2} = \frac{E(N_e + \delta N_e) + E(N_e - \delta N_e) - 2E(N_e)}{(\delta N_e)^2}, \tag{17}$$

where $E(N_e)$ is the ground-state energy when the number of electrons is N_e. The negative sign of χ_c indicates that the ground state is an insulator. The SC condensation energy ΔE_{SC} is finite for $0.05 \lesssim x \lesssim 0.2$. There is a coexistent metallic phase of SC and AF when $0.06 \lesssim x \lesssim 0.09$. The pure d-wave SC phase is in the range $0.09 \lesssim x \lesssim 0.2$. The typical energy scale of SC state is given by $\Delta E_{SC} \sim 0.005t$ and $\Delta_s \sim 0.01t$. The corresponding AF values are much larger than those of SC values. It has been shown that ΔE_{AF} is reduced when we improve the wave function from $\psi_\lambda = \psi_\lambda^{(1)}$ to $\psi_\lambda^{(3)}$ [48]. We here mention that the existence of AFI phase would depend on the value of t'. When t' is negative, the AFI phase will disappear as $|t'|$ increases.

4.3 Kinetic-energy driven superconductivity

In strongly correlated electron systems, the kinetic energy effect is important in determining the stable ground state. The kinetic energy effect in superconductivity has been examined for electronic models [103-112]. We discuss the role

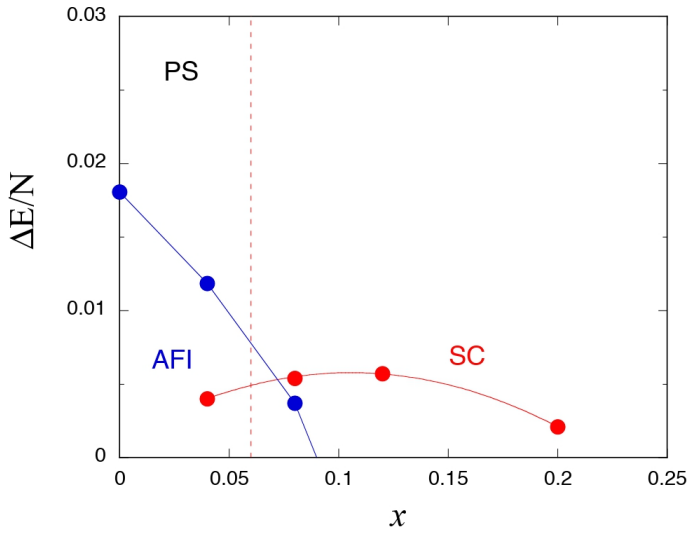

Figure 3. The condensation energy per site as a function of the hole doping rate x for the 2D Hubbard model on a 10×10 lattice (figure from [48] with a slight modification). The AF and SC condensation energies are shown. We set $t' = 0$ and $U/t = 18$. AFI indicates the AF insulating phase and SC shows the d-wave SC phase. At about $x \simeq 0.06$, the AF state changes from an insulator to a metallic state as x increases. We have the coexistent state of antiferromagnetism and superconductivity for $0.06 \lesssim x \lesssim 0.09$.

of the kinetic term in this subsection. For this purpose, we define two contributions to ΔE_{SC} from the kinetic term and the potential term, respectively:

$$\Delta E_{kin-sc} = E_{kin}(\Delta_s = 0) - E_{kin}(\Delta_s = \Delta_{s,\mathrm{opt}}), \tag{18}$$

$$\Delta E_{U-sc} = E_U(\Delta_s = 0) - E_U(\Delta_s = \Delta_{s,\mathrm{opt}}), \tag{19}$$

where E_{kin} and E_U are expectation values of the kinetic term K and the Coulomb term $U\sum_i n_{i\uparrow}n_{i\downarrow}$, respectively. From the definition we have

$$\Delta E_{SC} = \Delta E_{kin-sc} + \Delta E_{U-sc}. \tag{20}$$

In the BCS theory, the attractive interaction brings about superconductivity, and thus the interaction term V gives the SC condensation energy, that is, V in the SC state is lower than that in the normal state: $\delta V < 0$ (the variation of V is negative when the interaction is introduced). V will give the positive contribution to ΔE_{SC} This is also the case for weak coupling superconductivity. In fact, for the Gutzwiller-BCS wave function in the moderately correlated region, we have

$$\Delta E_{kin-sc} < 0, \quad \Delta E_{U-sc} > 0. \tag{21}$$

Instead, in the strongly correlated region where U is as large as $18t$, we obtain for ψ_λ as

$$\Delta E_{kin-sc} > 0, \quad \Delta E_{U-sc} < 0. \tag{22}$$

The kinetic part gives a positive contribution to ΔE_{SC}. We also define

$$\Delta E_{kin} = E_{kin}(\psi_G) - E_{kin}(\psi_\lambda) = E_{kin}(\lambda = 0) - E_{kin}(\lambda_{\rm opt}), \tag{23}$$

where $E_{kin}(\psi_G)$ and $E_{kin}(\psi_\lambda)$ are kinetic energies for ψ_G and ψ_λ, respectively. We show ΔE_{kin}, ΔE_{kin-sc} and ΔE_{SC} as well as E_U (the expectation value of the interaction term) in Fig. 4. In Fig. 4 we put $x = 0.12$ and $t' = 0$. The figure 4 shows that ΔE_{kin} changes its sign and begins to increase as U increases when $U \gtrsim 8t$. ΔE_{kin-sc} becomes positive in the strongly correlated region and shows a similar behavior to ΔE_{kin}. This behavior is consistent with the analysis for $Bi_2Sr_2CaCu_2O_{8+\delta}$ [103].

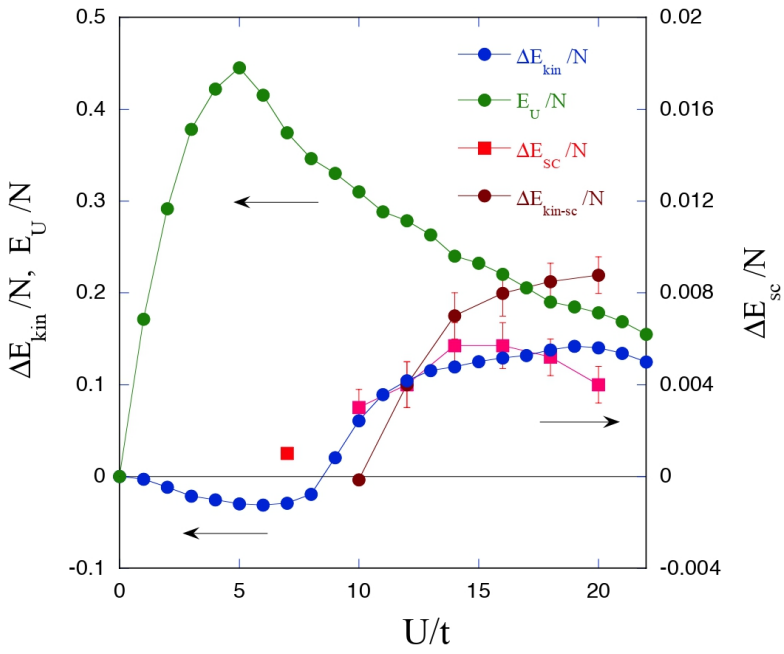

Figure 4. The kinetic-energy difference $\Delta E_{kin}/N$, the Coulomb energy E_U/N (left axis), the kinetic-energy gain $\Delta E_{kin-sc}/N$ and the SC condensation energy $\Delta E_{SC}/N$ (right axis) as a function of U/t on a 10×10 lattice where $N_e = 88$ and $t' = 0$ [102]. We use the periodic boundary condition in one direction and antiperiodic boundary condition in the other direction. The vertical axis on the right side shows the SC condensation energy $\Delta E_{SC}/N$ and the kinetic condensation energy $\Delta E_{kin-sc}/N$.

4.4 Nematic charge-ordered state and superconductivity

The existence of striped states has been pointed out by many authors in cuprate superconductors and in the 2D Hubbard model [43, 56-71]. We do not take into account the lattice effect here although it helps the formation of charge-ordered state. The charge and spin modulations are described as

$$\rho_i = \rho\cos\big(\boldsymbol{Q}_c\cdot(\boldsymbol{r}_i-\boldsymbol{r}_0)\big),\quad m_i = m\sin\big(\boldsymbol{Q}_s\cdot(\boldsymbol{r}_i-\boldsymbol{r}_0)\big), \tag{24}$$

where ρ and $m\equiv\Delta_{AF}$ are variational parameters for charge and spin modulations, respectively. $\boldsymbol{r}_0$ indicates the position of the domain boundary of spin modulation. For the commensurate AF state, we take $\boldsymbol{Q}_s=(\pi,\pi)$ and $\rho=0$. The stripe state is represented by incommensurate wave vector $\boldsymbol{Q}_s=(\pi\pm2\pi\delta,\pi)$ where δ stands for the incommensurability that is the inverse of the period of the AF order in the x-direction. In this state, two adjacent AF magnetic domains are separated by a one-dimensional domain wall in the y-direction. We have a π-phase shift when crossing a domain wall. For the charge modulation, we put $\boldsymbol{Q}_c=2\boldsymbol{Q}_s$ so that the charge modulation period is just half of the spin modulation period.

We consider the region with the doping rate given by $x\simeq 1/8$. The stripe state is usually most stable in this region. We consider, however, the large-U case where the AF order disappears as described above. In this case we have the ground state with charge order and without magnetic order for which $m=\Delta_{AF}=0$ and $\rho\neq0$. This state is called the nematic state. The calculation was carried out for $U/t=18$, $t'=0$ and $\delta=1/4$ (4-lattice charge periodicity) with the electron number $N_e=228$ on a 16×16 lattice. The charge-ordered nematic state is indeed stabilized for this set of parameters. We examine how superconductivity exists in the charge-ordered state. Let us consider the following gap function:

$$\Delta_{i,i+\hat{x}}=\Delta_s\cdot\left(1+\alpha\cos\left(\frac{1}{2}\pi x-\frac{\pi}{4}\right)\right),\quad \Delta_{i,i+\hat{y}}=-\Delta_s\cdot\left(1+\alpha\cos\left(\frac{1}{2}\pi x\right)\right), \tag{25}$$

where the coordinate of site i is $\boldsymbol{r}_i=(x,y)$ and α is a real parameter. The hole (or electron) rich domains exist at x = 4, 8, 12 and 16 for $\alpha>0$ (or $\alpha<0$). The gap function is spatially oscillating according to the charge modulation in this pairing state. In Fig. 5 we show the ground-state energy per site E/N as a function of Δ_s for the uniform d-wave state and the oscillating d-wave state. The result shows that the oscillating d-wave pairing state is most stable and will be realized. The superconducting state can coexist with inhomogeneous charge order with increased gap

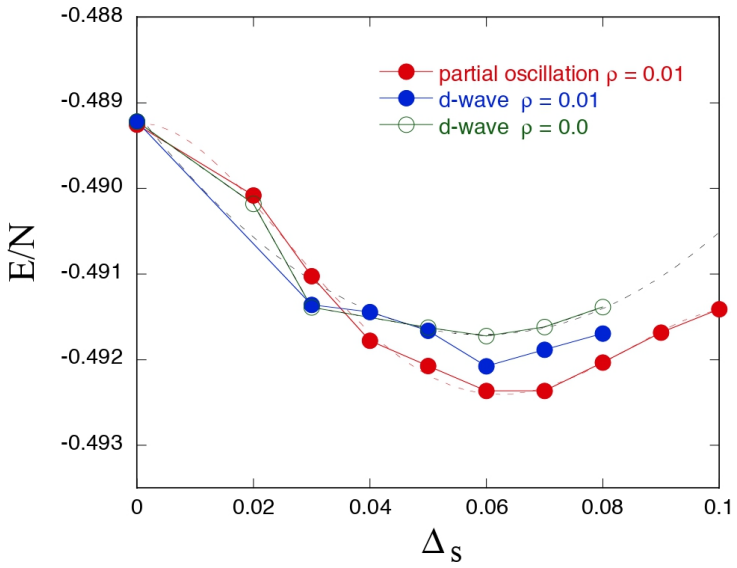

Figure 5. The ground-state energy per site as a function of the SC order parameter Δ_s for $U/t=18$ and $t'=0$ at $N_e=228$ on a 16×16 lattice. We used $g=0.005$, $\lambda=0.055$ and $\rho=0.01$. We compare three energy expectation values for the wave function with uniform d-wave symmetry with $\rho=0$ and 0.01, and that with partially oscillating d-wave pairing ($\alpha=-0.1$).

function. This gives a possibility that superconductivity is enhanced with higher T_c in cooperation with the inhomogeneous nematic charge ordering.

5. Superconductivity and strong correlation

In this section we examine the effect of strong correlation on superconductivity. We consider the effect of the Gutzwiller operator P_G on superconducting correlation function. The BCS wave function $\psi_{BCS}(\Delta_s)$ clearly shows the long-range correlation. In Fig. 6 we show the SC correlation function $D_{sc}(\ell) \equiv \langle \Delta^\dagger(i)\Delta(i+\ell)\rangle$, as a function of the lattice site for $N_e = 88$, $U = 18t$ and $t' = 0$ on a 10×10 lattice. Here the pair annihilation operator $\Delta(i)$ at the site i is defined by

$$\Delta(i) = \Delta_x(i) + \Delta_{-x}(i) - \Big(\Delta_y(i) + \Delta_{-y}(i)\Big), \tag{26}$$

where

$$\Delta_\alpha(i) = c_{i\downarrow}c_{i+\hat{\alpha}\uparrow} - c_{i\uparrow}c_{i+\hat{\alpha}\downarrow}, \tag{27}$$

for $\alpha = x$ and y. $\hat{\alpha}$ stands for the unit vector in the α-th direction.

The Fig. 6 shows that the pair correlation function for $U = 18t$ is almost constant when ℓ is large indicating that the ground state is superconducting. The values of $D_{sc}(\ell)$ for large ℓ are suppressed considerably compared to that for the non-interacting BCS wave function. This suppression is due to the strong correlation between electrons. This makes it rather hard to confirm the existence of superconducting phase in numerical calculations of pair correlation functions by, for example, quantum Monte Carlo calculations. In Fig. 7, we show the SC correlation function $D_{sc}(\ell)$ of $P_G\psi_{BCS}(\Delta_s)$ at the site $\ell = R_{max} = (5,5)$ with $i = (1,1)$ as a function of $1-g$ for $\Delta_s = 0.05t$ on a 10×10 lattice. R_{max} is the most distant point from the site $i = (1,1)$. The Fig. 7 indicates that the pair correlation function is suppressed by the electron correlation that is now given by the Gutzwiller on-site operator. Thus, we can say that the electron correlation has duality. This means that the electron correlation is an origin of attractive interaction between electrons and at the same time suppresses pair correlation functions.

The electron correlation has also an effect on the superconducting order parameter Δ. Δ is defined by

$$\Delta = \frac{1}{N}\sum_i \left(\langle c_{i\uparrow}^\dagger c_{i+\hat{x}\downarrow}^\dagger\rangle - \langle c_{i\uparrow}^\dagger c_{i+\hat{y}\downarrow}^\dagger\rangle\right). \tag{28}$$

We show Δ as a function of $1-g$ in Fig. 8. Δ exhibits a similar behavior to $D_{sc}(\ell)$, that is, Δ is reduced by P_G

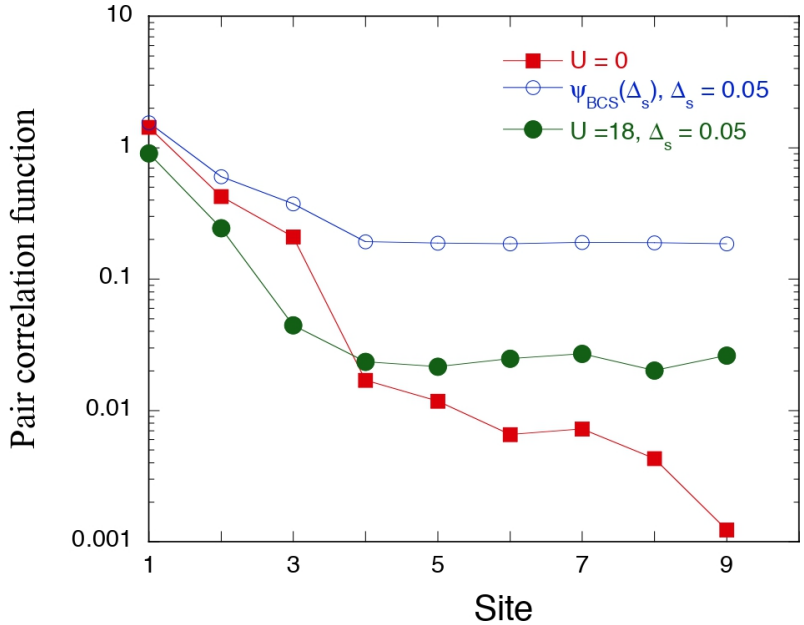

Fig. 6. The pair correlation function $D_{sc}(\ell)$ for $N_e = 88$, $U = 18t$ and $t' = 0$ on a 10×10 lattice where $i = (1,1)$ and $\ell = (1,1)$, $(1,2)$, $(1,3)$, $(1,4)$, $(1,5)$, $(2,5)$, $(3,5)$, $(4,5)$ and $(5,5)$. The figure includes $D_{sc}(\ell)$ for $U = 0$ (squares), that for the BCS wave function $\psi_{BCS}(\Delta_s)$ with $\Delta_s = 0.05t$ (open circles), and that for $U = 18t$ (filled circles).

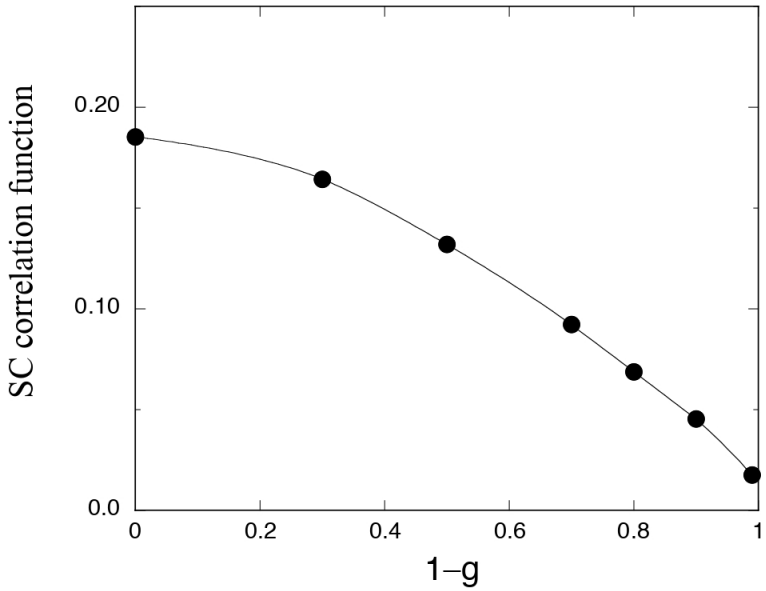

Fig. 7. The pair correlation function $D_{sc}(\ell)$ for $\ell = R_{max} = (5,5)$ of $P_G\psi_{BCS}(\Delta_s)$ with $\Delta_s = 0.05t$ on a 10×10 lattice. The parameter g is in the range of $0 \leq g \leq 1$ and $1 - g = 0$ corresponds to the BCS wave function.

when $g < 1$. Hence the electron correlation also leads to the reduction of the SC gap Δ. The strong electron correlation has duality, which means that the electron correlation becomes an origin of attractive interaction of *d*-wave pairing and at the same time, it suppresses SC correlation function and SC gap. One origin of this suppression is certainly the renormalization of the effective transfer integral and the effective mass. The heavy effective mass m^*/m reduces pair correlation functions and is not favorable for superconductivity as indicated by eq. (1). The exponential factor $e^{-\lambda K}$ could play a role to increase pair correlation by the kinetic energy effect.

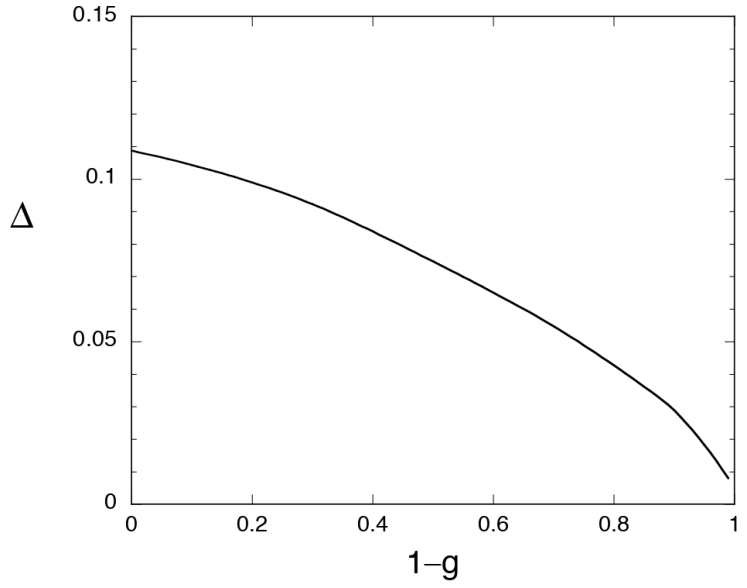

Fig. 8. The superconducting order parameter Δ as a function of $1 - g$ for $P_G\psi_{BCS}(\Delta_s)$ with $\Delta_s = 0.05t$ on a 10×10 lattice.

6. Discussion

The many-body wave function is important in the study of strongly correlated electron systems. We have constructed many-body wave functions starting from the Gutzwiller function to take into account strong correlation between electrons. The series $\psi_G, \psi_\lambda^{(1)} \equiv \psi_\lambda, \psi_\lambda^{(2)}, \psi_\lambda^{(3)}, \cdots$, will approach the exact wave function.

An instability toward magnetic ordering easily occurs in the two-dimensional Hubbard model. In particular, near the half-filled case with a small number of holes, the ground state has inevitably some magnetic or charge orders. Thus, we considered the strong correlated region where magnetic correlations and magnetic instabilities are suppressed.

Thus, we need a method of calculation by which we can evaluate physical properties in the strongly correlated region. This was the purpose of the study in this paper. We chose the value $U/t = 18$ in this paper. Since the extreme strong correlation reduces the pair correlation function, it is favorable that we can choose a moderate value of U being less than $U = 18t$. We expect that this value is reduced when we take account of further improved wave functions $\psi_\lambda^{(3)}$, $\psi_\lambda^{(4)}, \cdots$. In fact, the antiferromagnetic correlation is suppressed for the improved wave function $\psi_\lambda^{(3)}$[48]. We expect that this will lead to a superconducting state with larger gap function.

7. Conclusions

We have investigated the correlated superconducting state in the ground state of the two-dimensional Hubbard model based on the optimization variational Monte Carlo method. First, we discussed that the SC condensation energy obtained by numerical calculations is consistent with that estimated from experimental results for high-temperature cuprate superconductors. Second, we presented the phase diagram as a function of U based on improved many-body wave functions. The superconducting phase exists in the strongly correlated region where U is larger than the bandwidth. When $t' = 0$, the AF correlation weakens upon hole doping in the strongly correlated region and the pure d-wave SC is realized. Third, we have also shown the phase diagram as a function of the carrier density x, where basically there are three phases: antiferromagnetic insulating phase, metallic antiferromagnetic phase and superconducting phase. Fourth, then we discussed the kinetic energy effect that would assist the appearance of superconductivity and this effect may play an important role in the realization of high-temperature superconductivity. Fifth, we investigated cooperation of charge inhomogeneous order and superconductivity. This indicates the possibility that the superconducting critical temperature T_c will increase due to the coexistence with nematic charge ordering. Lastly, we showed the pair correlation function $D_{sc}(\ell)$. We discussed the effect of strong electron correlation on pair correlation function and SC order parameter. The pair correlation function is suppressed by the electron correlation operator P_G. Although the correlation function $D_{sc}(\ell)$ becomes small due to P_G, the long-range order still exists for ψ_λ.

Acknowledgments

The author expresses his sincere thanks to K. Yamaji and M. Miyazaki for fruitful discussions.

A part of computations was supported by the Supercomputer Center of the Institute for Solid State Physics, the University of Tokyo. The numerical calculations were also carried out on Yukawa-21 at the Yukawa Institute for Theoretical Physics in Kyoto University.

References

1. J. B. Bednorz, K. A. Müller. Z. Phys. B **1986**, 64, 189.
2. K. McElroy, R. W. Simmonds, J. E. Hoffman, D.-H. Lee, J. Orenstein, H. Eisaki, S. Uchida, J. C. Davis Nature **2003**, 422, 592.
3. N. E. Hussy, M. Abdel-Jawad, A. Carrington, A. P. Mackenzie, L. Balicas Nature **2003**, 425, 814.
4. C. Weber, K. Haule, G. Kotliar Phys. Rev. B **2008**, 78, 134519.
5. M. S. Hybertsen, M. Schluter, N. E. Christensen Phys. Rev. B **1989**, 39, 9028.
6. H. Eskes, G. A. Sawatzky, L. F. Feiner Physica C 1989, 160, 424.
7. A. K. McMahan, J. F. Annett, R. M. Martin Phys. Rev. B **1990**, 42, 6268.
8. H. Eskes, G. Sawatzky Phys. Rev. B **1991**, 43, 119
9. V. J. Emery Phys. Rev. Lett. **1987**, 58, 2794.

10. J. E. Hirsch, E. Y. Loh, D. J. Scalapino, S. Tang Phys. Rev. B **1989**, 39, 243.
11. R. T. Scalettar, D. J. Scalapino, R. L. Sugar, S. R. White Phys. Rev. B **1991**, 44, 770.
12. A. Oguri, T. Asahata, S. Maekawa Phys. Rev. B **1994**, 49, 6880.
13. S. Koikegami, K. Yamada J. Phys. Soc. Jpn. **2000**, 69, 768.
14. T. Yanagisawa, S. Koike, K. Yamaji Phys. Rev. B **2001**, 64, 184509.
15. S. Koikegami, T. Yanagisawa J. Phys. Soc. Jpn. **2001,** 70, 3499.
16. T. Yanagisawa, S. Koike, K. Yamaji Phys. Rev. B **2003**, 67, 132408.
17. S. Koikegami, T. Yanagisawa Phys. Rev. B **2003**, 67, 134517.
18. S. Koikegami, T. Yanagisawa J. Phys. Soc. Jpn. **2006**, 75, 034715.
19. T. Yanagisawa, M. Miyazaki, K. Yamaji J. Phys. Soc. Jpn. **2009**, 78, 031706.
20. C. Weber, A. Lauchi, F. Mila, T. Giamarchi Phys. Rev. Lett. **2009**, 102, 017005.
21. B. Lau, M. Berciu, G. A. Sawatzky Phys. Rev. Lett. **2011**, 106, 036401.
22. C. Weber, T. Giamarchi, C. M. Varma Phys. Rev. Lett. **2014**, 112, 117001.
23. A. Avella, F. Mancini, F. Paolo, E. Plekhano Euro. Phys. J. B **2013**, 86, 265.
24. H. Ebrahimnejad, G. A. Sawatzky, M. Berciu J. Phys. Cond. Matter **2016**, 28, 105603.
25. S. Tamura, H. Yokoyama Phys. Procedia **2016**, 81, 5.
26. T. Yanagisawa, M. Miyazaki, K. Yamaji EPL **2021**, 134, 27004.
27. J. Hubbard Proc. Roy. Soc. London **1963**, 276, 238.
28. J. Hubbard Proc. Roy. Soc. London **1964**, 281, 401.
29. M. C. Gutzwiller Phys. Rev. Lett. **1963**, 10, 159.
30. S. Zhang, J. Carlson, J. E. Gubernatis Phys. Rev. B **1997**, 55, 7464.
31. S. Zhang, J. Carlson, J. E. Gubernatis Phys. Rev. Lett. **1997**, 78, 4486.
32. T. Yanagisawa, Y. Shimoi Int. J. Mod. Phys. B **1996**, 10, 3383.
33. T. Yanagisawa, Y. Shimoi, K. Yamaji Phys. Rev. B **1995**, 52, R3860.
34. T. Nakanishi, K. Yamaji, T. Yanagisawa J. Phys. Soc. Jpn. **1997**, 66, 294.
35. K. Yamaji, T. Yanagisawa, T. Nakanishi, S. Koike Physica C **1998**, 304, 225.
36. K. Yamaji, T. Yanagisawa, S. Koike Physica B **2000**, 284-288, 415.
37. K. Yamaji, T. Yanagisawa, M. Miyazaki, R. Kadono J. Phys. Soc. Jpn. **2011**, 80, 083702.
38. T. M. Hardy, P. Hague, J. H. Samson, A. S. Alexandrov Phys. Rev. B **2009**, 79, 212501.
39. T. Yanagisawa, M. Miyazaki, K. Yamaji J. Mod. Phys. **2013**, 4, 33.
40. N. Bulut Advances in Phys. **2002**, 51, 1587.
41. H. Yokoyama, Y. Tanaka, M. Ogata, H. Tsuchiura J. Phys. Soc. Jpn. **2004**, 73, 1119.
42. H. Yokoyama, M. Ogata, Y. Tanaka J. Phys. Soc. Jpn. **2006**, 75, 114706.
43. M. Miyazaki, T. Yanagisawa, K. Yamaji J. Phys. Chem. Solids **2002**, 63, 1403.
44. T. Yanagisawa New J. Phys. **2008**, 10, 023014.
45. T. Yanagisawa New J. Phys. **2013**, 15, 033012.
46. T. Yanagisawa, S. Koike, K. Yamaji J. Phys. Soc. Jpn. **1998**, 67, 3867
47. T. Yanagisawa J. Phys. Soc. Jpn. **2016**, 85, 114707.
48. T. Yanagisawa J. Phys. Soc. Jpn. **2019**, 88, 054702.
49. T. Yanagisawa Condens. Matter **2019**, 4, 57.
50. R. M. Noack, S. R. White, D. J. Scalapino EPL **1995**, 30, 163.
51. R. M. Noack, N. Bulut, D. J. Scalapino, M. G. Zacher Phys. Rev. B **1997**, 56, 7162.
52. K. Yamaji, Y. Shimoi, T. Yanagisawa Physica C **1994**, 235, 2221.
53. S. Koike, K. Yamaji, and T. Yanagisawa J. Phys. Soc. Jpn. **1999**, 68, 1657.
54. K. Yamaji, K. Harigaya, T. Yanagisawa, Y. Shimoi J. Phys. Soc. Jpn. **1992**, 61, 3689.

55. T. Nakano, K. Kuroki and S. Onari Phys. Rev. B **2007**, 76, 014515.
56. J. M. Tranquada, J. D. Axe, N. Ichikawa, Y. Nakamura, S. Uchida, B. Nachumi Phys. Rev. B **1996**, 54, 7489.
57. T. Suzuki, T. Goto, K. Chiba, T. Shinoda, T. Fukase, H. Kimura, K. Yamada, M. Ohashi, Y. Yamaguchi Phys. Rev. B **1998**, 57, R3229.
58. K. Yamada, C. H. Lee, K. Kurahashi, J. Wada, S. Wakimoto, S. Ueki, H. Kimura, Y. Endoh, S. Hosoya, G. Shirage, J. Birgeneau, M. Greven, M. A. Kastner, Y. J. Kim Phys. Rev. B **1998**, 57, 6165.
59. M. Arai, T. Nishijima, Y. Endoh, T. Egami, S. Tajima, K. Tomimoto, Y. Shiohara, M. Takahashi, A. Garrett, S. M. Bennington Phys. Rev. Lett. **1999**, 83, 608.
60. H. A. Mook, P. Dai, F. Doga, R. D. Hunt Nature **2000**, 404, 729.
61. S. Wakimoto, R. J. Birgeneau, M. A. Kastner, Y. S. Lee, R. Erwin, P. M. Gehring, S. H. Lee, M. Fujita, K. Yamada, Y. Edoh, K. Hirota, G. Shirane Phys. Rev. B **2000**, 61, 3699.
62. A. Bianconi, N. L. Saini, A. Lanzara, M. Missori, T. Rossetti, H. Oyanagi, H. Yamaguchi, K. Oka, T. Ito Phys. Rev. Lett. **1996**, 76, 3412.
63. M. Kato, K. Machida, H. Nakanishi, M. Fujita J. Phys. Soc. Jpn. **1990,** 59, 1047.
64. T. A. Maier, G. Alvarez, M. Summers, T. C. Schulthess Phys. Rev. Lett. **2010**, 104, 247001.
65. R. Mondaini, T. Ying, T. Paiva, R. T. Scalettar Phys. Rev. B **2012**, 86, 184506.
66. A. Bianconi Nature Phys. **2013**, 9, 536.
67. H. Yamase, Y. Sakurai, M. Fujita, S. Wakimoto, K. Yamada Nature Commun. **2021**, 12, 2223.
68. M. Miyazaki, T. Yanagisawa Phys. Lett. A **2022**, 446, 128276.
69. T. Yanagisawa, S. Koike, M. Miyazaki, K. Yamaji J. Phys. Condens. Matter **2001**, 14, 21.
70. T. Ying, R. Mondaini, X. D. Sun, T. Paiva, R. M. Fye, R. T. Scalettar Phys. Rev. B **2014**, 90, 075121.
71. S. Yang, T. Ying, W. Li, J. Yang, X. Sun, X. Li J. Phys. Condens. Matter **2021**, 33, 115601.
72. J. E. Hoffman, K. McElroy, D.-H. Lee, K. M. Lang, H. Eisaki, S. Uchida, J. C. Davis Science **2002**, 295, 466.
73. W. D. Wise, M. C. Boyer, K. Chatterjee, T. Kondo, T. Takeuchi, H. Ikuta, Y. Wang, E. W. Hudson Nature Phys. **2008**, 4, 696.
74. T. Hanaguri, C. Lupien, Y. Kohsaka, D.-H. Lee, M. Azuma, M. Takano, H. Takagi, J. C. Davis Nature **2004**, 430, 1001.
75. M. Miyazaki, T. Yanagisawa, K. Yamaji J. Phys, Soc. Jpn. **2009**, 78, 043706.
76. A. Valletta, A. Bianconi, A. Perali, N. L. Saini Z. Physik B Condensed Matter **1997,** 104, 707.
77. P. M. Shirage, K. Kihou, K. Miyazawa, C.-H. Lee, H. Kito, H. Eisaki, T. Yanagisawa, Y. Tanaka, A. Iyo Phys. Rev. Lett. **2009**, 103, 257003.
78. T. Yanagisawa, K. Odagiri, I. Hase, K. Yamaji, P. Shirage, Y. Tanaka, A. Iyo, H. Eisaki J. Phys. Soc. Jpn. **2009**, 78, 094718.
79. A. Perali, D. Innocenti, A. Valletta, A. Bianconi Superconduct. Sci.Technol. **2012**, 25, 124002.
80. A. Perali, A. Bianconi, A. Lanzara, N. L. Saini Solid State Commuu. **1996**, 100, 181.
81. A. Bianconi, A. Valletta, A. Perali, N. L. Saini Physica C **1998**, 296, 269.
82. F. V. Kusmatsev, D. Di Castro, G. Bianconi, A. Bianconi Phys. Lett. A **2000**, 275, 118.
83. K. A. Müller, G. M. Zao, K. Conder, H. Keller J. Phys. Condens. Matter **1998**, 10, L291.
84. A. Bianconi Solid State Commun. **1994**, 91, 1.
85. L. F. Feiner, J. H. Jefferson, R. Raimondi Phys. Rev. B **1996**, 53, 8751.
86. K. Kuroki, S. Onari, R. Arita, H. Usui, Y. Tanaka, H. Kontani, H. Aoki Phys. Rev. Lett. **2008**, 101, 087004.
87. N. Grewe, F. Steglich Handb. Phys. Chem. Of Rare Earths **1991**, 14,343.
88. A. C. Hewson The Kondo Problem to Heavy Fermions **1993**, Cambridge University Press, Cambridge UK.
89. Y. Onuki Physics of Heavy Fermions: Heavy Fermions and Strongly Correlated Electron Systems **2018**, World Scientific Pub Co Inc., Singapore.
90. T. Ishiguro, K. Yamaji, G. Saito Organic Superconductors **2012**, Springer, Berlin, Germany.
91. R. Akashi, M. Kawamura, S. Tsuneyuki, Y. Nomura, R. Arita Phys. Rev. B **2015**, 91, 224513.
92. H. Otsuka J. Phys. Soc. Jpn. **1992**, 61, 1645.
93. T. Yanagisawa, S. Koike, K. Yamaji J. Phys. Soc. Jpn. **1999**, 68, 3608.
94. D. Eichenberger, D. Bäriswyl Phys. Rev. B **2007**, 76, 180504.
95. D. Bäriswyl, D. Eichenberger, M. Menteshashvii New J. Phys. **2009**, 11, 075010.
96. D. Bäriswyl J. Supercond. Novel Magn. **2011**, 24, 1157.
97. T. Yanagisawa, M. Miyazaki EPL **2014**, 107, 27004.

98. P. W. Anderson Science **1987**, 235, 1196.
99. T. Yanagisawa Phys. Rev. B **2007**, 75, 224503.
100. K. G. Wilson Rev. Mod. Phys. **1975**, 47, 773.
101. J. W. Loram, K. A. Mirza, J. R. Cooper, W. Y. Liang Phys. Rev. Lett. **1993**, 71, 1740.
102. Z. Hao, J. R. Clem, M. W. McElfresh, L. Civale, A. P. Malozemoff, F. Holtzberg Phys. Rev. B **1991**, 43, 2844.
103. Th. A. Maier, M. Jarrell, A. Macridin, C. Slezak Phys. Rev. Lett. **2004**, 92, 027005.
104. M. Ogata, H. Yokoyama, Y. Yanase, Y. Tanaka, H. Tsuchiura J. Phys. Chem. Solids **2006**, 67, 37.
105. E. Gull, A. J. Millis Phys. Rev. B **2012**, 86, 241106.
106. L. F. Tocchio, F. Becca, S. Sorella Phys. Rev. B **2016**, 94, 195126.
107. S. Feng Phys. Rev. B **2003**, 68, 184501.
108. P. Wrobel, R. Eder, R. Micnas J. Phys. Condens. Matter **2003**, 15, 2755.
109. H. Guo, S. Feng Phys. Lett. A **2007**, 361, 382.
110. T. Yanagisawa, M. Miyazaki, K. Yamaji Condensed Matter **2021**, 6, 12.
111. T. Yanagisawa Phys. Lett. A **2021**, 403, 127382.
112. G. Deutscher, A. F. Santander-Syro, N. Bontemps Phys. Rev. B **2005**, 72, 092504.